Ocean wave climate in the Mediterranean Sea

Wassim Seksaf
Msc. GGL
2022-2023

Supervisors:
Mr. Wayne Crawford
Mr. Xavier Bertin

Table of Contents

ABSTRACT:

The earth's normal modes undergo a continuous low-level vibration referred to as the seismic "hum", yet its precise origin remains a subject of ongoing scientific investigation. Current research suggests that infragravity waves, long-period (25-250 s) ocean surface gravity waves generated through wave-wave interactions in coastal zones, may represent the strongest potential source of this phenomenon. Seafloor seismological networks, which are progressively gaining prevalence, seafloor stations are almost always equipped with a pressure sensor, and as the deep ocean infragravity waves generate significant seafloor pressure fluctuations, it is therefore possible to use seismological noise measurements to study the behaviour of IG waves and other ocean wave phenomena. For the first time, in this study our aim is to establish a correlation between infragravity waves and seismological noise using seafloor seismological network and sea-surface wave hindcasts and a nearby weather buoy situated in a "small" basin — the Mediterranean Sea —. Additionally, we seek to correlate infragravity waves from the seafloor data with wave parameters from the surface data and use these correlations to propose forcing parameters.

Introduction:

Seismic "hum" is low-level but continuous excitation of earth's normal modes from 0.001 to 0.02 Hz. This hum is several orders of magnitude smaller than the better-known microseism peak in global seismological data, but it is important because: 1) it may reveal temporal variations in Earth's deep structure; 2) it may mask other seismological/environmental signals; and 3) it may provide valuable information about oceanic infragravity waves, which can generate coastal hazards.

The source of seismic "hum" is the subject of ongoing research, but one of the strongest potential sources are infragravity ("IG") waves (e.g., Bertin et al., 2018): ocean surface gravity waves with much longer periods (25–250 s) than typical wind-generated ocean surface waves. IG waves are generated in coastal zones through wave-wave interactions or oscillation of the breaking point (Webb et al 1991). IG waves are strongly correlated with ocean swell, indicating that IG waves are driven by swell (Munk et al 1949, Tucker et al 1950). IG waves can generate dangerous harbour seiches and coastal flooding and may control the dynamics of tidal inlets.

Seismological noise measurements have been used to study the behaviour of IG waves and other ocean wave phenomena. The link between IG waves and ocean seismological noise is an important area of research for understanding the complex interactions between the ocean and the Earth's surface. A recent model for the generation and propagation of these waves reproduces the general noise trends observed on land stations, but not the exact noise levels (Ardhuin et al., 2014, 2015). IG waves are difficult to measure at the sea surface because of their relatively small size, but easier to measure at the seafloor because their long wavelength leaves their pressure signal relatively unattenuated with depth. A better understanding of the generation and variability of IG waves requires broad seafloor measurement networks.

Large seafloor seismological networks are becoming more and more common, as technological advances and cost reductions allow longer and better-quality seafloor data, near to many important geodynamic elements (subduction zones, mid-ocean ridges, intraplate volcanoes, near-shore faults…). Seafloor seismological sensors detect not only earthquake arrivals, but also environmental, biological, and human phenomena (storms, whale calls and shipping, for example). The stations are almost always equipped with a pressure sensor to separate signals and to provide complementary information. For example, broadband sensors can measure the ground deformation caused by IG wave loading (Crawford et al., 1991). Although deep ocean IG waves are generally quite small (1-10 mm), they generate significant seafloor pressure fluctuations because higher-frequency ocean wave energy is hydrodynamically filtered out. (Webb, S. C., and W. Crawford (1999)).

In this report we use a seafloor seismological network, combined with sea-surface wave hindcasts and a nearby weather buoy from a "small" basin — the Mediterranean Sea — to study the generation of deep ocean IG waves. Larger (oceanic) basins have a large domain of potential noise sources, which makes correlating wave energy and its noise

sources more challenging. Within a smaller basin, waves generally form quickly and locally, which should simplify correlating IG waves and seismological noise. We correlate infragravity waves from the seafloor data with wave parameters from the surface data and use these correlations to propose forcing parameters.

Study area:

The Mediterranean area is the collision zone between the European and African plates. The Mediterranean basin comprises several geodynamic regions affected by different seismic activity on a predominantly West-East axis.

The recent AlpArray experiment (2017-2018) was a multinational collaboration to tomographically image the deep structure of the Alps. A complete ray coverage required stations in the sea (red circles, Figure 1) as well as on land. We use stations from this seafloor network for our study.
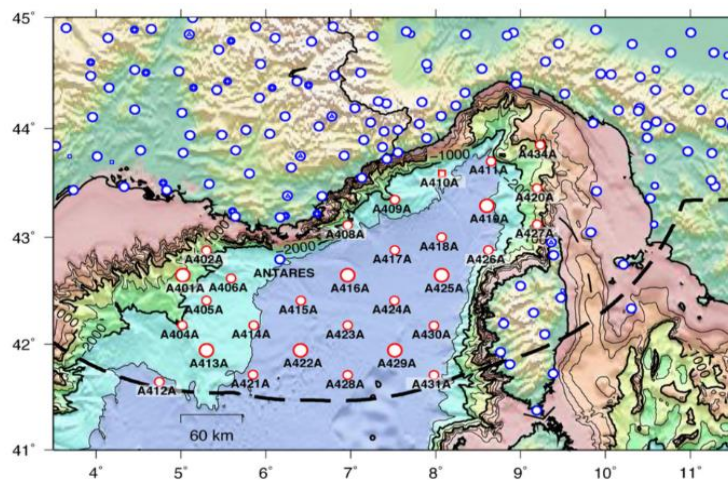
Figure 1 Map of the AlpArray OBS network in the Ligurian Sea (June 2017- February 2018). Large circles indicate broadband OBSs, small circles indicate DEPAS OBS with wideband sensors.

We focus on the low frequency pressure data collected by several seafloor stations located between the southern French coast and Corsica. The data are from differential pressure gauges, whose passband is from about 0,002 Hz to 50 Hz. We calculate sea surface IG wave levels from this data, then correlate them with 1) data collected from a wave rider buoy located offshore Corsica, and 2) the output of a regional wave model calculated using the WAVE WATCH III software package.
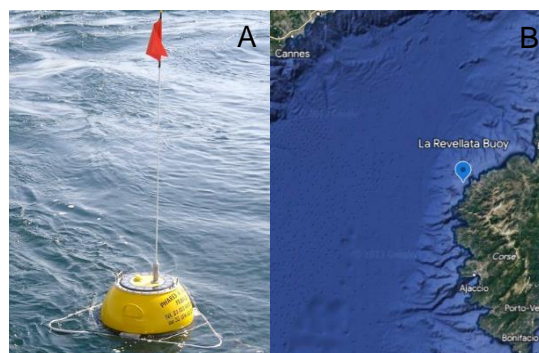
Figure 2 (A) The "La Revellata" waverider buoy deployed offshore Corsica at 130m water depth (B) the location of the buoy.

Methodology:

Ocean bottom seismometer data:

The broad-band Ocean bottom seismometers (OBSs) used in this study contain a 3-component seismometer and a differential pressure gauge (DPG). We use the DPG data, which is the most sensitive to ocean waves. The data are stored in the SeisComp Data Structure (SDS) used by seismological data centres and the metadata (instrument position, response, etc) are stored in StationXML format used by these same data centres. We extract the DPG data using a python package (Obspy, https://docs.obspy.org) then calculate 1h power spectral densities (Decibel (dB)), over a period of 8 months for most stations and over 2-3 months for some other stations that had a shorter time coverage.
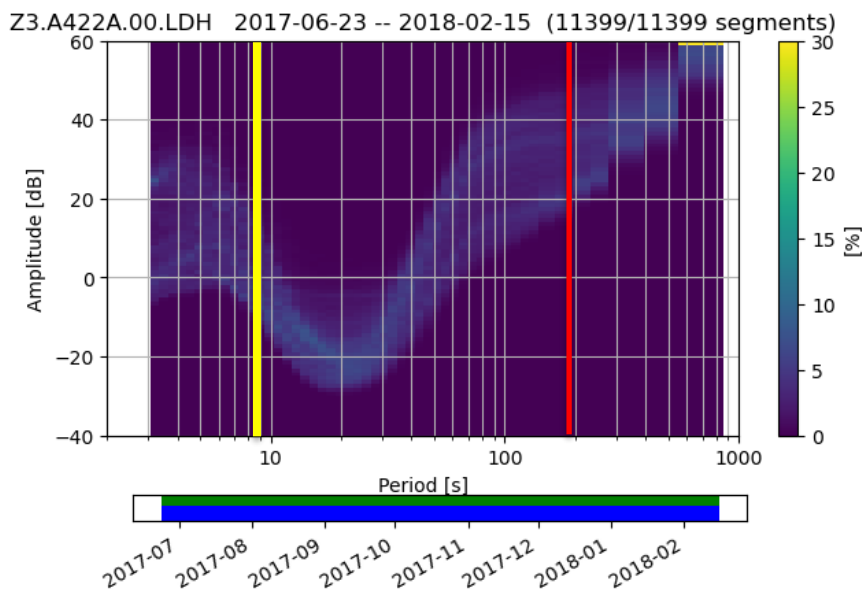
Figure 3 Pressure Power Spectrum Density (PPSD) for the DPG data collected from the station A422A for 8 months with the yellow line representing the end of the Microseims band and the red line representing the begening of the IG band

To simplify processing, we first determined and selected the time period with the overall highest-pressure amplitude. We used a time-series plot (Figure 4a) and a spectrogram (Figure 4b) of signal power to analyse and visualize the signal variations. The spectrogram represents the power of different frequency components over time. The figures show that the highest infragravity wave pressure amplitudes are found at the end of autumn and the beginning of winter (red vertical lines, Figure 4A). We therefore focus on this time period for our analysis.
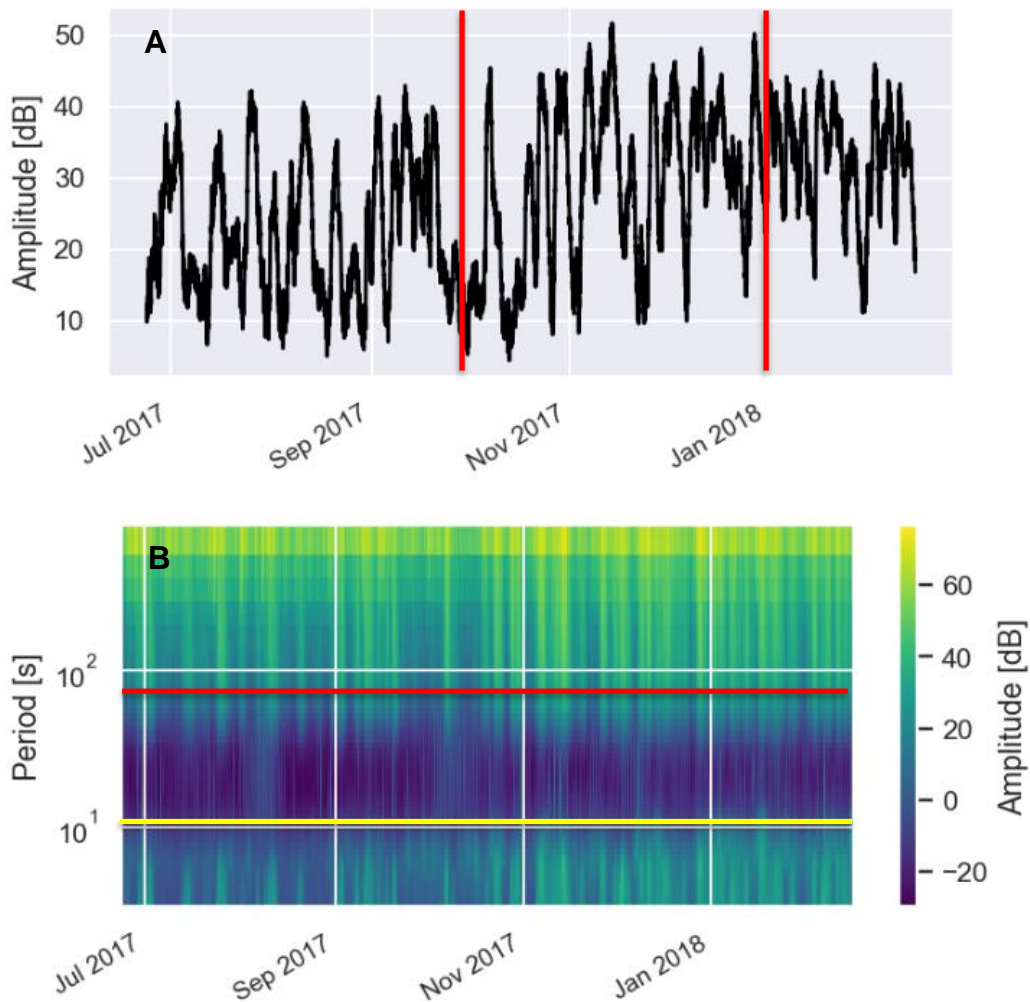
Figure 4 (A) Amplitude variations over the 8-month experiment period. The period of highest amplitudes lies between the 2 red vertical lines. (B) Spectrogram representing the frequency content of the signal over time. The yellow lines span the end of the Microseims band, and the red lines the beginning of the IG band

In the deep ocean, DPGs measure the pressure difference between the outside and an internal reference chamber whose pressure is close to that at the seafloor, using a capillary leak to slowly equilibrate. These gauges provide readings in Pa, but the Power Spectral densities are given in decibels (dB) referred to 1 Pascal per square root Hertz (1 Pa/sqrt (Hz)). The following formula converts the readings from dB (reference 1 Pa/sqrt (Hz)) to pressure in Pa/sqrt (Hz):

$$P = 10^{\left(\frac{L}{20}\right)}$$

where P represents the reading in decibels and L represents the corresponding pressure value in Pa/sqrt (Hz). The result of this conversion is shown in Figure 5:
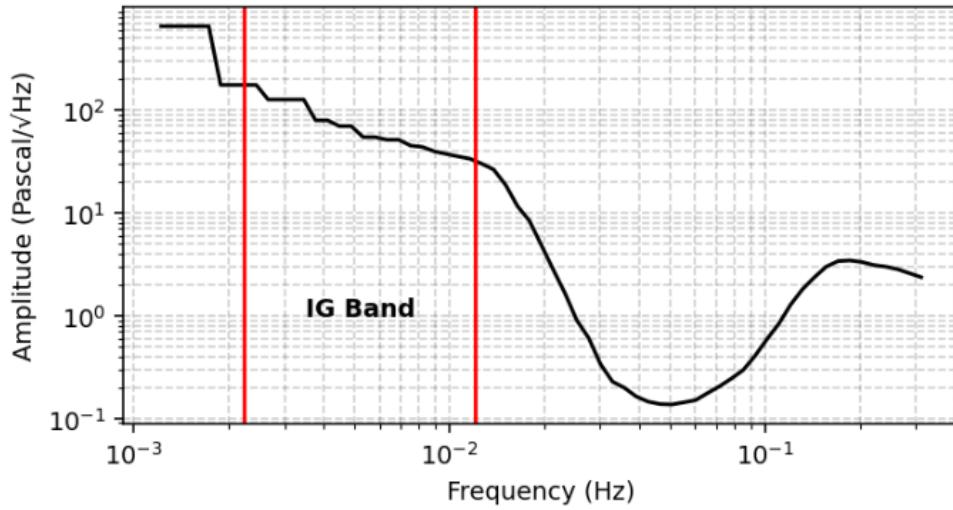
Figure 5 DPG bottom spectrum represented along the frequency axes with the IG band represented between the 2 vertical red lines.

Figure 5 shows that the spectral level is highest towards lower frequencies, which is explained by the long wavelength of infragravity waves at these periods. As the frequency decreases, the influence of these waves becomes more dominant due to their large wavelengths and thus cover a broader frequency range, leading to a significant increase in the spectral level towards lower frequencies during their interaction with the seafloor. To estimate the surface height of these waves, we propagate the seafloor-measured IG wave signal (in Pa) to the sea-surface IG wave amplitude (in m), using the relationship between sea-surface and sea-floor pressure for ocean surface gravity waves and a water depth H (Webb, S. C., and W. C. Crawford (1991)):

$$Pb = \rho g \zeta / cosh(kh)$$

Where Pb represents the bottom pressure values, ζ the surface wave height, g the gravitational acceleration, k the wavenumber, h the depth of the instrument and ρ the water density. We solve this equation for ζ, meaning that we must multiply the bottom pressure by cosh(kh).
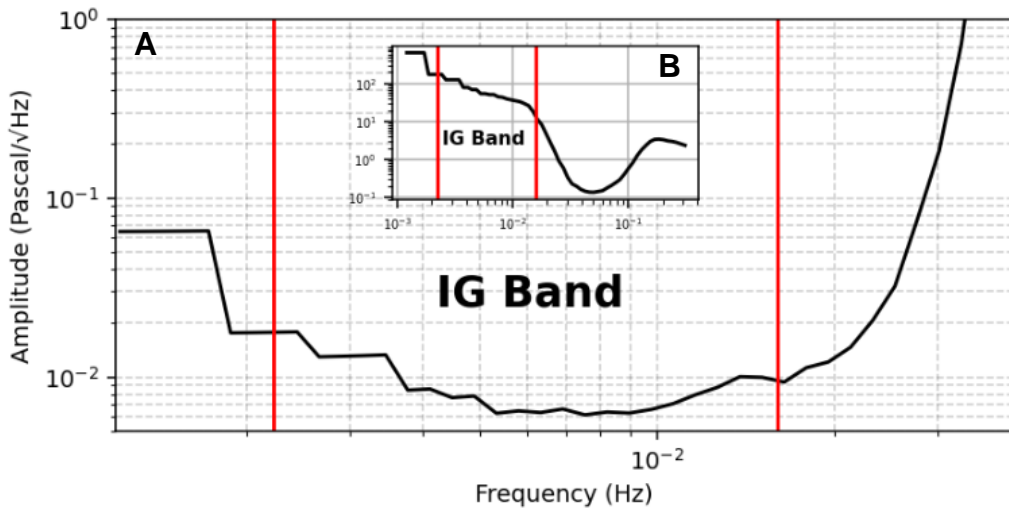
Figure 6 (A) previous figure of the DPG bottom spectrum. (B) Zoom in on the IG band after multiplying the spectrum by the cosh

The problem with multiplying the seafloor signal by cosh(kh) is that cosh(kh) increases exponentially with higher frequencies. Therefore, once the signal is dominated by noise or signals other than infragravity waves, the "surface amplitude" explodes. We therefore limit our analysis to frequencies where the "surface amplitude" is approximately flat with frequency (0.003-0.015 Hz in the Figure 6, 0.003-0.012 Hz for the ensemble of seafloor stations). Finally, we integrated these values over the frequency band from 0.003 to 0.012 Hz to obtain the sea-surface IG wave amplitude (Figure 7).
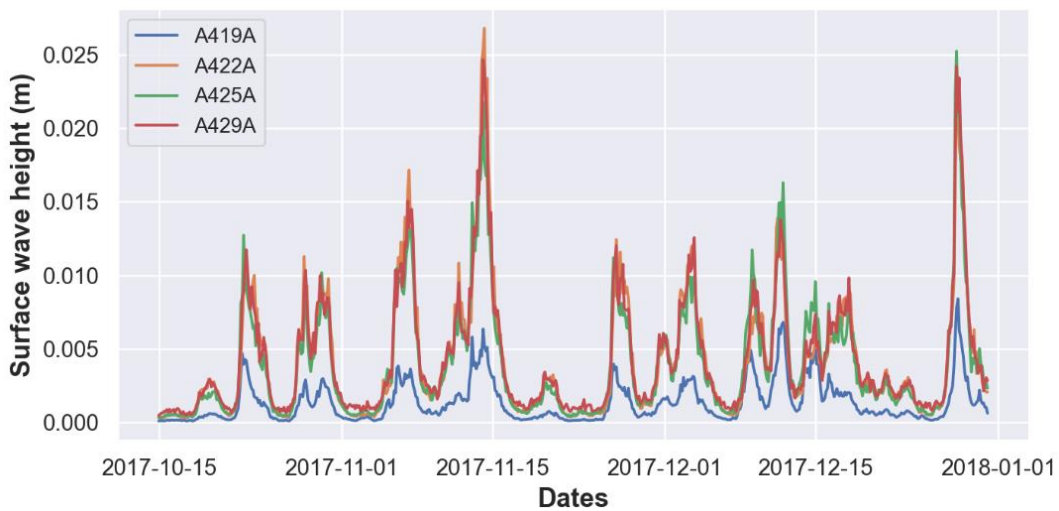
Figure 7 Surface wave heights computed from the DPG data of 4 stations in the IG band using the equation (2)

The surface wave height refers to the vertical distance between the crest (highest point) and trough (lowest point) of a surface ocean wave. It is a measure of the amplitude of the wave and is often used to describe the size of waves observed on the ocean surface.

Buoy collected data:

We use buoy data to validate the prediction of the numerical model (Wave Watch III) and to correlate with the DPG time series. We used data from a Buoy named "La Revellata" located at 42°34.150' N latitude and 08°39.000' E longitude, near to the Corsican coastal city of Corsica. The data are available from 02/05/2013 to 30/04/2023. The raw data are sent by radio link to a receiving station on land, where they are recorded, validated, and broadcast in real time whenever possible. The measurements are also recorded on a memory card inside the equipment, to limit data loss due to transmission problems.
For this project, we will take the same period as the DPG dataset. The significant wave heights for this period are shown in Figure 8.
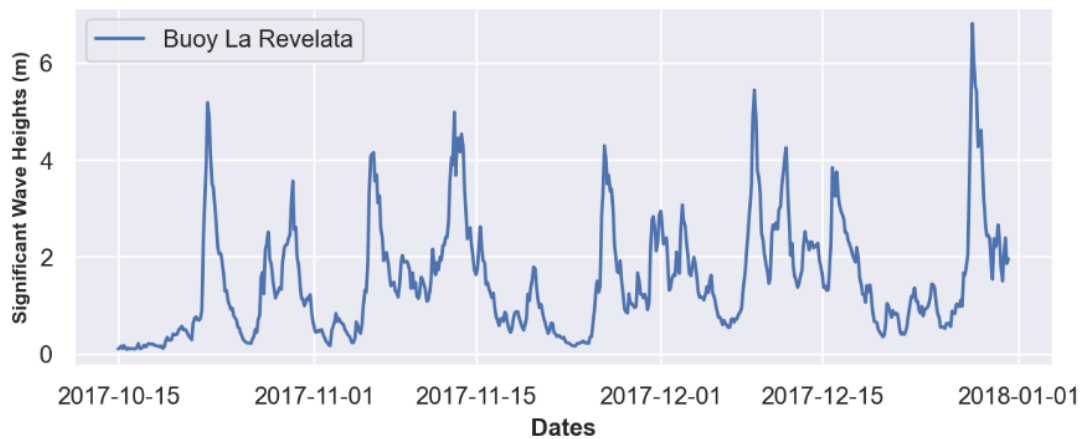
Figure 8 Significant wave heights from "La Revellata" buoy

Wave Watch III data:

WaveWatch III is a wave model used to simulate and predict waves in the oceans. Developed by the National Oceanic and Atmospheric Administration (NOAA), WaveWatch III is widely regarded as one of the most advanced wave modelling systems. It provides valuable information for coastal engineering, and climate research. WaveWatch III utilizes a numerical approach to forecast wave characteristics such as height, period, direction, and spectral information. The model considers a multitude of complex factors that influence wave behaviour, including wind speed and direction, water depth, atmospheric pressure.

In this study we ran the model for a period of time from "2017-10-15 03:00:00" to "2017-12-31 03:00:00". The main elements of the WWIII configuration for this run are Code version 6.07, regular grid with resolution of 0.02° (~2 km), ERA5 wind field forcing parameter, "test 475" source terms described by (Alday et al 2021). We compare the output at 4 OBS stations [A419A, A422A, A425A, A429A].

The figure below is the representation of the significant wave hights predicted at the 4 stations using the Wave Watch III model:
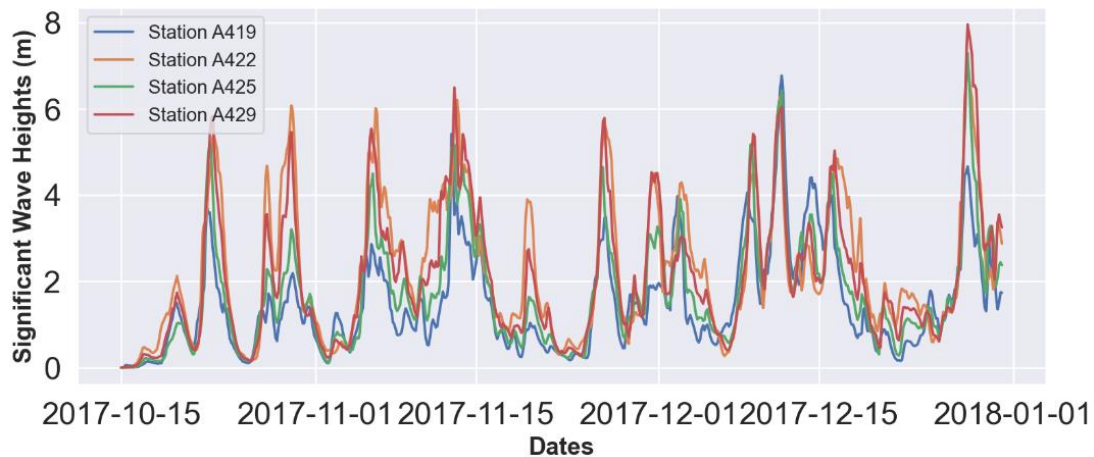
Figure 9 Significant wave heights from the model WaveWatch III

IG waves either appear as "free" (Herbers et al 1994) or "bound" (Herbers et al 1995). When wind blows over the water surface, it transfers energy to the water through frictional forces. This energy is then transformed into wave motion, creating free wind waves. These waves serve as the primary source for wave energy in the ocean, and through nonlinear interactions, they can generate "bound" waves that contribute to the complex wave dynamics observed along coastal regions. "Bound" waves correspond to the non-linear interactions between waves and can have very long wavelengths and very low (IG waves) or double (microseisms) frequencies.

Bound IG waves generally generate significant seafloor energy in shallow water (<20m), but almost none at greater depths (Webb et al., 1991; Herbers and Guza, 1991, 1992). At greater depths, the IG waves are observed to be free (obeying the linear wave equations, not the non-linear terms). The transformation from bound to free IG waves is still debated, but the most common theory is that the IG waves are freed when their higher frequency carriers (the wind waves) break at coastlines, generating the well-known lower frequency surf beat (Herbers et al 1995).

To investigate the source of the IG waves, we calculate the bound IG wave using the directional 1D spectrum from WW III and Longuet-Higgins theory. We then see how well these bound waves correlate with the DPG-measured IG waves. If they are highly correlated, then the measured IG waves may be bound waves. If not, they are probably free IG waves.

To convert the WW III spectrum into a free surface time series we use the SWASH software, which is a general-purpose numerical tool for simulating unsteady, non-hydrostatic, free-surface, rotational flow and transport phenomena in coastal waters as driven by waves, tides, buoyancy, and wind forces. It provides a general basis for describing wave transformations from deep water to a beach.

The equation that we used is:

$$\zeta_b = a_0 + \sum_{j=1}^{N} a_j * \cos(\omega_j t - \varphi_j)$$

Where ζ_b is the surface elevation signal of the incident wave, N is the number of Fourier components, a_0 is the mean water level, and a_j, ω_j and φ_j are the amplitude, angular frequency, and local phase lag, respectively.

For a given wave spectrum $E(\omega)$, a time series can be synthesised by calculating the amplitude of each harmonic, as follows (M. Zijlema et al 2011):

$$a_j = \sqrt{2E(\omega_j)\Delta\omega}$$

Using these 2 equations, we generate 1h free surface time series (Figure 10):
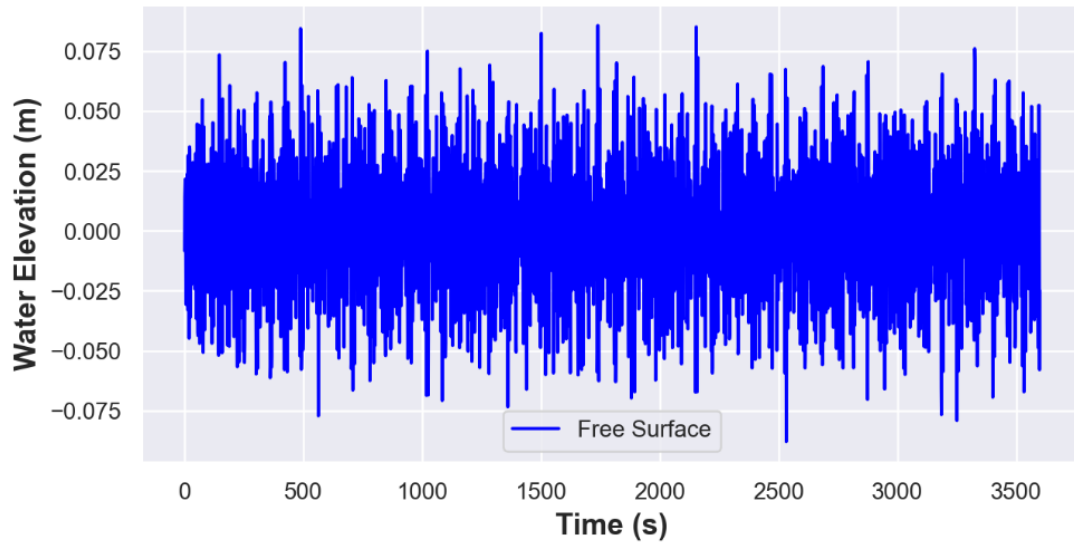
Figure 10 Free Surface time series generated from 1D spectrum for an Hs=6.1m and Tp =12s for 1 hour

We then compute the bound waves from the calculated free surface times series using the 1D equation from (Longuet-Higgins and Stewart 1962):

$$\eta(x,t) = \frac{-S_{xx}(x,t)}{\rho(gh - c_g^2)} + K$$

12

Where S_{xx} is the wave radiation stress, which corresponds to the momentum flux associated with short waves, h is the mean water depth, ρ is the water density, g is the gravitational acceleration, cg is the short waves group velocity and K is a constant.

Results and Discussion:

Basic hydrodynamic statistics:

To validate the WW III results, first we selected the closest DPG station to La Revelata buoy which is station A225A at 2708m water depth. We compare the prediction of the model with the buoy data by computing the bulk parameters, including significant wave height (Hs), mean wave period (Tm02), and peak wave period (Tp).

The figure bellow shows the different time series computed for each of the bulk parameters and their correlation coefficient with respect to the buoy values:
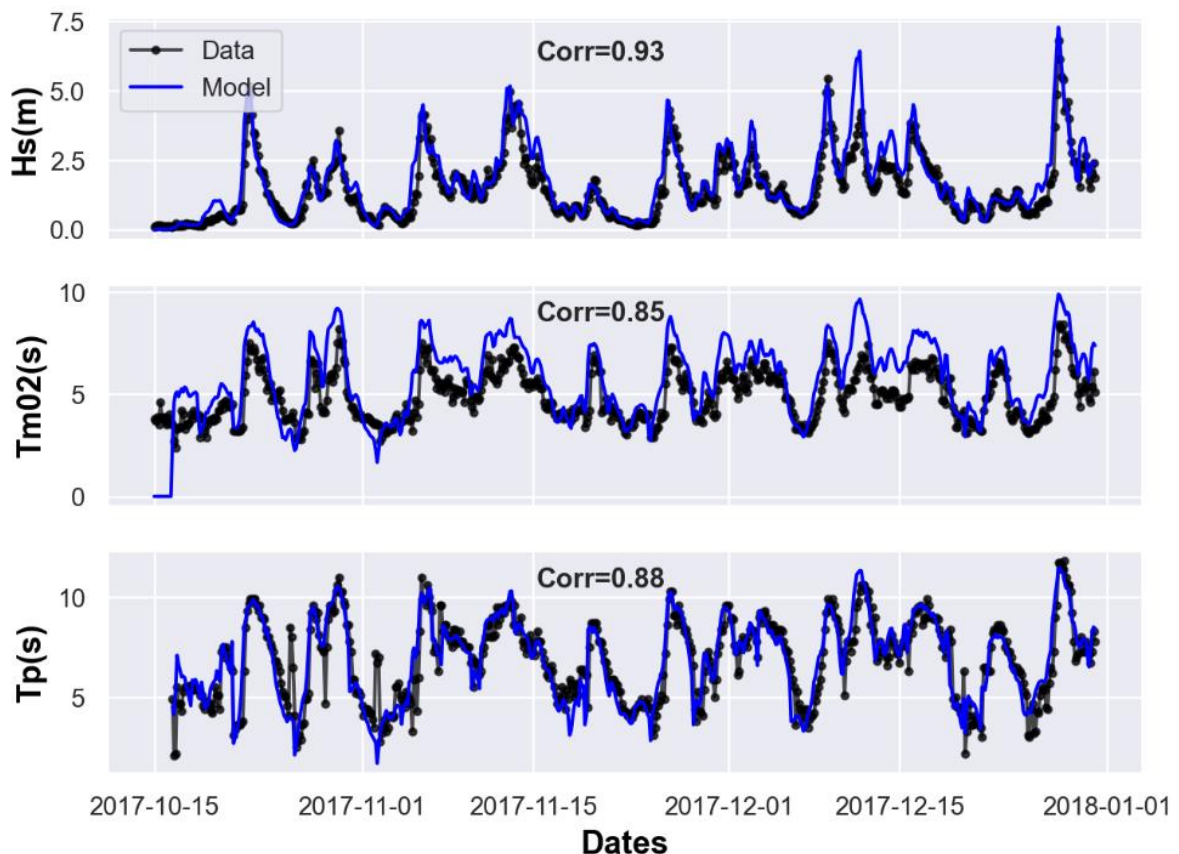
Figure 11 Representation of the comparison between the different bulk parameters calculated for the model output in blue and for the buoy data observation in black.

The result indicates a good agreement between the model's output and the actual measurements from the buoys, the strong correlation shows that the model's predictions align closely with the actual measurements from the buoys. It confirms that the model is capable of reproducing the observed waves variations at an overall 88% accuracy.

To understand and explain the IG wave times series that we computed from the seafloor station DPG data, we compare them with the WW III and Buoy Hs time series (Figure 12).
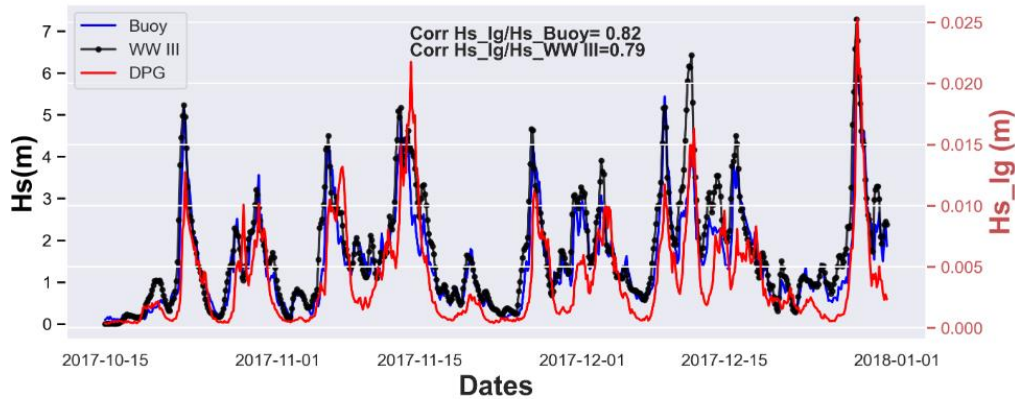
Figure 12 Time series comparison between the 3 datasets, in Red the HS in the IG band from DPG data. In Blue the Hs time series from the Buoy observation data. In Black the Hs time series from WW III output. With their respective correlation coefficients

Figure 12 shows a strong correlation between the IG waves and the wave pairs at sea swell frequencies, especially at some spikes (for example the 28[th of] December 2017 where we measure the highest value in both frequencies band), indicating a strong relationship between these waves.

A study conducted by (Ardhuin et al. 2014) discovered a strong correlation between infragravity wave height in deep water and a parameter that combines both wave height and mean wave period. Interestingly, their findings revealed that the largest infragravity wave heights were also associated with the largest mean wave period, rather than being solely dependent on the height of the sea swell waves only. We therefore compared the IG waves with all three of these parameters (Figure 13).
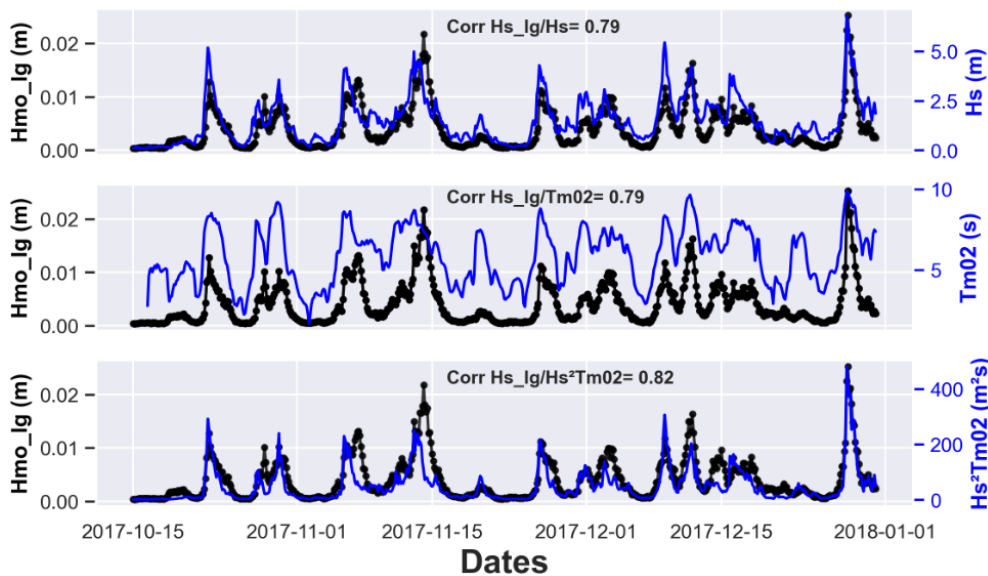
Figure 13 Comparison of IG waves significant wave height with swell sea waves bulk parameters (Hs/Tm02) and Ardhuin study parameter Hs²Tm02

The correlation is indeed highest between IG waves the combination of wave height and mean wave period, in agreement with (Arduin et al. 2014).

Two main mechanisms for IG wave generation have been identified. The theoretical work of (Biésel 1952), further expanded upon by (Longuet-Higgins and Stewart 1962) and (Hasselmann 1962), elucidated that these waves can originate in areas far from the shore, well beyond the surf zone. The underlying process involves complex interactions between pairs of waves with sea-swell frequencies, leading to the emergence of IG waves.

Herbers et al (1995) showed that free IG waves heights are very much related to the wind and sea swell waves heights Hs. To determine if in our case IG waves are "free" (Herbers et al 1994) or "bound" (Herbers et al 1995), we will therefore compute the bound wave from the WW III 1D spectrum and compare the spectrum significant wave height of IG (Hmo_Ig) to the bound wave spectrum significant wave height (Hmo_Bw).

Bound wave:

In natural settings, the short-wave field consists of various random elements. As a result of sub-harmonic interactions, these components undergo a process whereby a spectrum of bound wave components is forced to emerge (Bertin et al 2018), following the mechanisms elucidated by (Hasselmann et al 1962) and (Herbers et al 1994).The resulting bound waves, exhibit frequencies typically ranging from 0.004 to 0.04 Hz and possess amplitudes that are relatively small, often measured in centimetres, particularly in deeper water. In this part, we will calculate the bound wave using the (Longuet-Higgins and Stewart 1962) equation.

Figure 14 shows a 1 hour bound wave signal (red line) derived from the free surface signal derived from one 1D WW III spectrum:
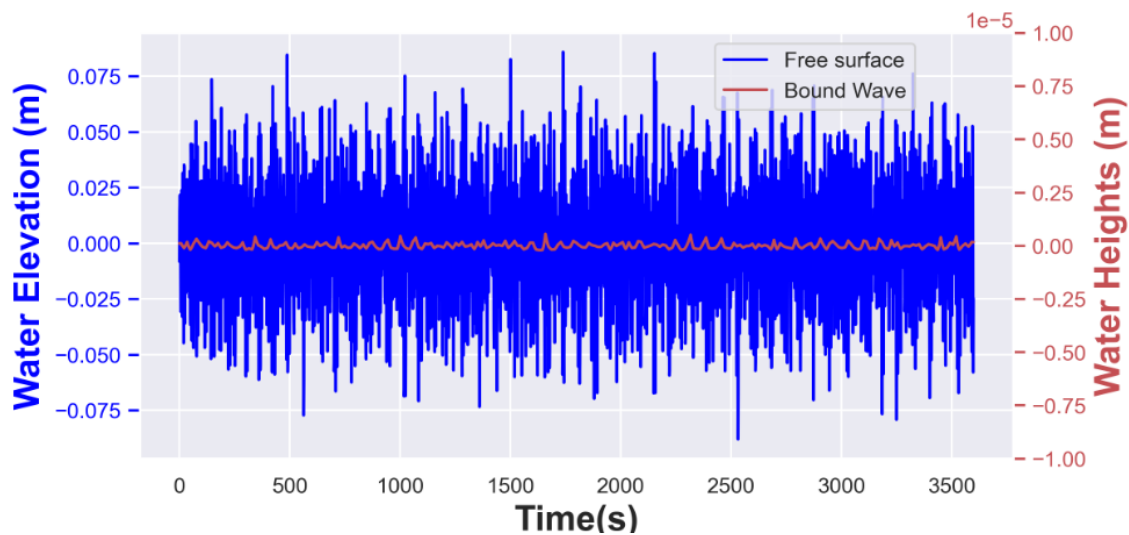
Figure 14 Resulting free surface elevation (blue) and bound wave (red) as computed according to Longuet-Higgins and Stewart (1962).

We calculated the bound wave for all the time periods, then calculated the bound waves' significant wave heights and to compare the result with the IG wave heights (Figure 15).
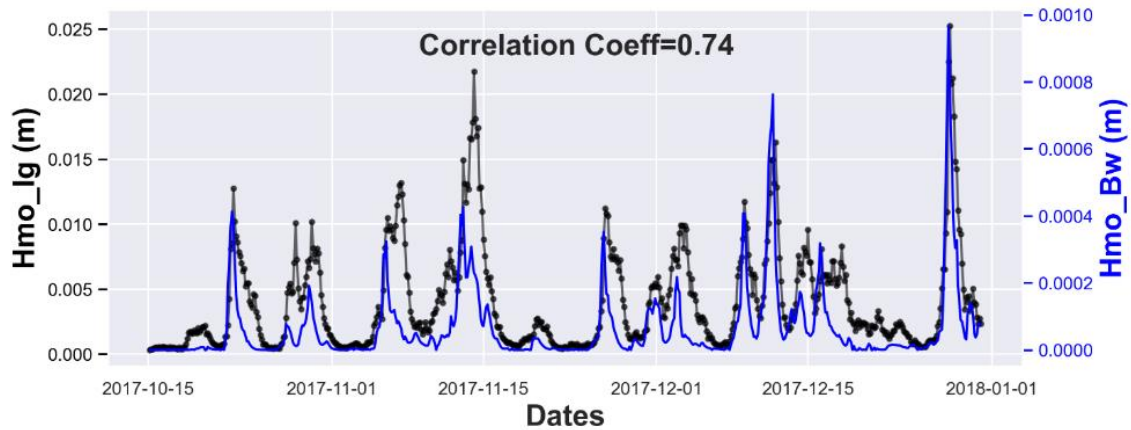
Figure 15 Comparison of the Hmo_Ig computed for the station A425A with the Hmo_Bw of the bound wave computed from WW III 1D spectrum for the same station.

There is a similarity between both the series, but 1) the measured waves are larger, and 2) the measured waves "last" longer. This suggests that the measured waves are "free" waves, which agrees with very limited coastal measurements indicating that free waves dominate at depths greater than ~20 m (Webb et al., 1991; Herbers and Guza, 1991, 1992).

The Longuet-Higgins approach is only valid for a flat bottom and does not account for wave spreading. It therefore tends to overestimate Hmo_Bw, but this does not invalidate our results because they already predict lower and briefer bound waves than the measured IG waves. (Hasselmann 1962 and Herbers et al 1994) proposed a two-dimensional extension of the model proposed by (Longuet-Higgins and Stewart 1962) that takes into consideration wave spreading, but the calculations were too complicated to implement and validate in the scope of this study.

Perspectives:

I)

If we compare our results with the "MARC LOPS" WW III models (https://marc.ifremer.fr/), focusing for example on the biggest spike of Hs in our time series (28 December 2017) we can see (Figure 16) that the wave direction towards the Corsica coast. Calculating the wave group velocity and the distance between the station and the coast, we calculate a travel time of two hours for the bound wave arrive to travel from the station to the coast. If we look closely at Figure 15, there is a strong correlation between Hmo_Ig and Hmo_Bw at the beginning of each energy spike, which could be explained by the theory of (Herbers et al 1995) that the bound wave breaks at coastlines and generates the IG free wave that will then propagate with a velocity of √gH and, as we are in deep water, comes back to the station almost instantly.
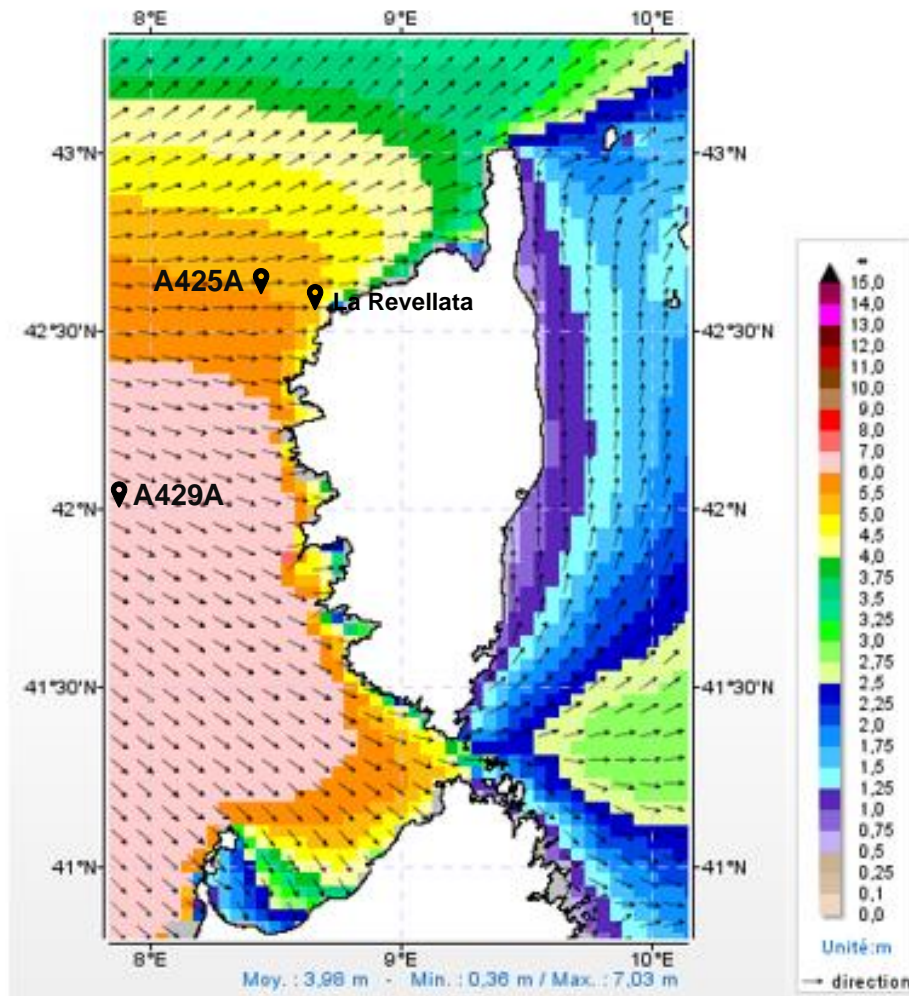
Figure 16 Offshore Corsica map of significant waves heights and waves direction for the 28th of December 2017 with approximation of the nearest stations

II)

Another improvement to this study would be to compute the bound wave using the Hasselman theory that considers the wave spreading. This should reduce the bound wave Hmo amplitudes and so will not contradict our results but may provide more insight into the relationship between bound waves and the start of the IG waves observed at the seafloor.
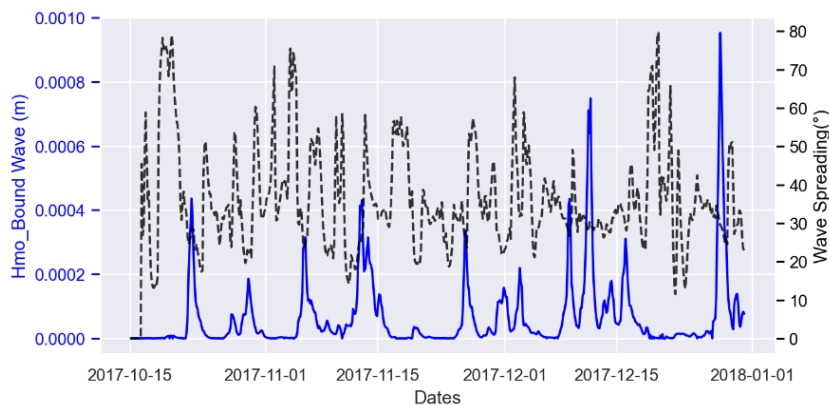
Figure 17 Representation of the wave spreading (°) with the variation of the bound wave amplitudes in (m)

Conclusion

Through the project workflow, we first identified the different frequency bands on the seismological noise signal and then, using signal processing tools, we correlated this noise with the IG waves in their specific frequency band.

We then used the "La Revelata" buoy dataset to validate the Wave Watch III ("WW III") numerical model: the correlation coefficient ranges from 82% to 93%.

Finally, we used the WW III output significant wave heights to study the forcing parameters and the sources of the IG waves computed from the DPG data. We find that the highest IG waves amplitudes are recorded during the highest swell and that their onset correlates with the predicted generation of bound IG waves, but that their amplitudes are higher and they last longer. This suggest that they are free waves which are probably generated from bound waves at coastlines. Finally, the measured IG waves are better correlated with the surface wave height squared times the wave period Tm02 than with the surface wave height, the surface wave height squared or the wave period. These results, measured in a relatively small basin, support the results and models proposed by Herbers et al (1995) and Arduin et al. (2014), based on data from much larger ocean basins.

Bibliography and references:

- Alday, M., Accensi, M., Ardhuin, F., & Dodet, G. (2021). A global wave parameter database for geophysical applications. Part 3: Improved forcing and spectral resolution. Ocean Modelling, 166, 101848.

- Ardhuin, F., Rawat, A., & Aucan, J. (2014). A numerical model for free infragravity waves: Definition and validation at regional and global scales. Ocean Modelling, 77, 20-32.

- Ardhuin, F., Gualtieri, L., & Stutzmann, E. (2015). How ocean waves rock the Earth: Two mechanisms explain microseisms with periods 3 to 300 s. Geophysical Research Letters, 42(3), 765-772.

- Bertin, X., de Bakker, A., Van Dongeren, A., Coco, G., André, G., Ardhuin, F., ... & Tissier, M. (2018). Infragravity waves: From driving mechanisms to impacts. Earth-Science Reviews, 177, 774-799.

- Biésel, F (1952) "General Equations of Second Order for Irregular Waves," La Houille Blanche, 38:3, 372-376,

- Crawford, W., Ballu, V., Bertin, X., & Karpytchev, M. (2015). The sources of deep ocean infragravity waves observed in the N orth A tlantic O cean. Journal of Geophysical Research: Oceans, 120(7), 5120-5133.

- Munk, W. H. (1949). Wave action on structures. Transactions of the AIME, 179(01), 11-28.

- Longuet-Higgins, M. S., & Stewart, R. W. (1962). Radiation stress and mass transport in gravity waves, with application to 'surf beats'. Journal of Fluid Mechanics, 13(4), 481-504.

- Hasselmann, K. (1962). On the non-linear energy transfer in a gravity-wave spectrum Part 1. General theory. Journal of Fluid Mechanics, 12(4), 481-500.

- Hasselmann, K., Munk, W., & MacDonald, G. J. F. (1963). Bispectra of ocean waves. In Symposium on Time Series Analysis (pp. 125-139). New York.

- Herbers, T. H. C., & Guza, R. T. (1991). Wind-wave nonlinearity observed at the sea floor. Part I: Forced-wave energy. Journal of physical oceanography, 21(12), 1740-1761.

- Herbers, T. H. C., & Guza, R. T. (1992). Wind-wave nonlinearity observed at the sea floor. Part II: Wavenumbers and third-order statistics. Journal of physical oceanography, 22(5), 489-504.

- Herbers, T. H. C., Elgar, S., Guza, R. T., & O'Reilly, W. C. (1992). Infragravity-frequency (0.005-0.05 Hz) motions on the shelf. In Coastal Engineering 1992 (pp. 846-859).

- Herbers, T. H. C., & Guza, R. T. (1994). Nonlinear wave interactions and high-frequency seafloor pressure. Journal of Geophysical Research: Oceans, 99(C5), 10035-10048.

- Herbers, T. H. C., Elgar, S., Guza, R. T., & O'Reilly, W. C. (1995). Infragravity-frequency (0.005–0.05 Hz) motions on the shelf. Part II: Free waves. Journal of physical oceanography, 25(6), 1063-1079.

- Rawat, A., Ardhuin, F., Ballu, V., Crawford, W., Corela, C., & Aucan, J. (2014). Infragravity waves across the oceans. Geophysical Research Letters, 41(22), 7957-7963.

- Tucker, M. J. (1950). Surf beats: Sea waves of 1 to 5 min. period. Proceedings of the Royal Society of London. Series A. Mathematical and Physical Sciences, 202(1071), 565-573.

- Webb, S. C., Zhang, X., & Crawford, W. (1991). Infragravity waves in the deep ocean. Journal of Geophysical Research: Oceans, 96(C2), 2723-2736.

- Webb, S. C., & Crawford, W. C. (1999). Long-period seafloor seismology and deformation under ocean waves. Bulletin of the Seismological Society of America, 89(6), 1535-1542.

- Zijlema, M., Stelling, G., & Smit, P. (2011). SWASH: An operational public domain code for simulating wave fields and rapidly varied flows in coastal waters. Coastal Engineering, 58(10), 992-1012.

- https://marc.ifremer.fr/

- https://docs.obspy.org

- http://www.alparray.ethz.ch/en/seismic_network/obs/overview/